DOI: 10.17725/rensit.2020.12.349

Synthesis and Characterization of Thin Nanostructured Bismuth Doped Tin Oxide Films and Sensing Studies

Andrey V. Smirnov, Vladimir V. Kolesov, Iren E. Kuznetsova
Kotelnikov Institute of Radioengineering and Electronics of RAS, http://www.cplire.ru/
Moscow 125009, Russia
E-mail: andre-smirnov-v@yandex.ru, kvv@cplire.ru, kuziren@yandex.ru
Ilya V. Sinev, Vyacheslav V. Simakov
N.G. Chernyshevskii Saratov State University, https://www.sgu.ru/
Saratov 410012, Russian Federation
E-mail: sineviv@gmail.com, viatcheslav.simakov@gmail.com
Received Juni 08, 2020; peer reviewed Juni 22, 2020; accepted Juni 30, 2020

Abstract: **The tin dioxide (SnO_2) films doped with bismuth by means of magnetron sputtering of semiconductor two-phase target and powder BiO_2 as source of Bi were produced. The effect of bismuth dope concentration variation on the microstructure, electrophysical and gas-sensing properties was investigated. It has been found, that films consist of crystalline rods with diameter of 21±2 nm and length of 120±10 nm. Bismuth doping provided decrease in signal timing drift of acetone sensor in analyzed probe. Sensitivity to acetone vapor of the sample derived from targets with 0.01% bismuth oxide concentration increase almost by 10 times (up to 850) in comparison with undoped film at 300°C. Based on the obtained experimental data the mechanism of bismuth dope influence on electrical and gas-sensing properties of produced tin dioxide films was evaluated. Obtained results have shown capability the use of bismuth doped dioxide tin films for development of saturated acetone vapor sensors.**

Keywords: **Tin dioxide, bismuth doping, gas-sensor, films morphology, saturated acetone vapors**

UDC 539.23, 539.25, 681.586

Acknowledgements: The work was carried out within the framework of the state task from Ministry of Science and Higher Education #0030-2019-0016 and was partially supported by Russian Foundation of Basic Research, projects #19-07-00300 and #20-37-70021. Andrey Smirnov thanks for financial support Council of Grants of the President of the Russian Federation. (Project # MK-1503.2020.8).

For citation: Andrey V. Smirnov, Ilya V. Sinev, Viacheslav V. Simakov, Vladimir V. Kolesov, Iren E. Kuznetsova. Synthesis and Characterization of Thin Nanostructured Bismuth Doped Tin Oxide Films and Sensing Studies. *RENSIT*, 2020, 12(3):349-360. DOI: 10.17725/rensit.2020.12.349.

Contents

1. INTRODUCTION

Tin dioxide (SnO_2) is one of the most promising semiconducting materials for production of sensory layers of gas sensors. However, this material contains a large quantity of intrinsic defects of crystal lattice resulting in irreversible changes in its properties at extreme temperature variations. Furthermore, sensing film of pure SnO_2 has low sensibility and weak selectivity to variety of gases. Therefore pure SnO_2 slightly using in sensors production [1, 2]. Catalytic electroactive dopants as In, Pd, Ni, Er, Zn are used for correction of pure SnO_2 physicochemical properties, particularly, for intrinsic defects compensation, structure strengthening, selectivity and sensibility improvement [3-7]. Tin dioxide thin films doping provides significant modification their microstructure and electronic structure changing crystallites growth mechanisms and parameters, producing additional donor and acceptor states hence changing material conductance. As well SnO_2 doping with various additives Pt, Pd, Au is able to change material lattice constant. [8-11].

There are a lot of papers devoted to investigation of influence of various dopants to SnO_2 film on the gas sensor parameters. Deposition of Pd nanoparticles on the SnO_2 film surface results in sensor operation temperature reducing down to room temperature [12]. SnO_2 doped with cerium showed an increase in the sensor sensitivity to hydrogen sulfide [13, 14] and various organic gases [15]. Cobalt, ruthenium, nickel or iron doping significantly increases tin dioxide sensitivity to methane, trimethylamine, and ethanol, respectively [16-19]. The use of SnO_2 films doped with zirconium leads to decrease in the sensor operating temperature and increase of the maximum sensitivity to ethanol, acetone, and isopropyl alcohol vapor [20]. It is known that introduction of Cu dopant into SnO_2 film leads to decrease the drift of the sensor baseline while the material selectivity to H_2S increases comparing with CO and C_2H_5OH [21-24]. In [25] it has been shown that donor-like sites created during the deposition of SnO_2:Cu film provide much better sensor stability than intrinsic donors in pure SnO_2 films. The effect can be explained by a decrease in the mobility of oxygen vacancies when coupled with Cu atoms vacancies. It has been supposed that in the case of bismuth doping it is possible to realize such mechanism. However, due to the much larger ionic radius of Bi (1.03A) than that of tin (0.69A), when the complex is formed with an oxygen vacancy, the compound will create a greater strain in the crystal structure. This will lead to a more effective inhibition of migration of oxygen vacancies and, consequently, to greater stability of the gas sensor.

In earlier it was shown that Bi doping changed the structural and phase characteristics of SnO_2 films [26, 27]. Usually, bismuth oxide powder is used as a target to produce films doped with bismuth. Introduction of bismuth oxide permit to control crystallite size in a wide range. The increasing bismuth oxide concentration from 0 to 20 mol.% leads to average crystallite size decreases in twice. It has been also shown possibility to create a resistive sensor based on bismuth oxide branched SnO_2 nanowires with selectively sensitivity to NO_2 [28]. However, there is practically no research of Bi effect on SnO_2 film morphology. As well the review of the literature has been shown that the study of the possibility of using SnO_2 films doped with bismuth as sensory coatings for acetone sensor is small compared with other dopants. In this regard, we studied nanostructured thin films of SnO_2 doped with bismuth and their sensitivity to acetone vapors.

2. EXPERIMENTAL PROCEDURE

2.1. Semiconductor film sample producing

The tin dioxide thin films under study were prepared using the method of high-frequency magnetron sputtering of a dielectric target by means a set up Orion-40T VTC-PVD-600 (South Korea). The circle targets with bare SnO_2 powder and with mixed SnO_2 and BiO_2 powders were obtained by dry pressing. Five targets were prepared: pure tin dioxide, and tin dioxide with BiO_2 additives with concentration of 0.01, 0.1, 1, and 10 mass.%. The diameter and the thickness of the targets were equal to 100 mm and 4 mm, respectively. Sputtering was carried out in an argon atmosphere with the addition of oxygen in a flow ratio of 3:1, respectively. Polished polycore plates and monocrystalline silicon wafers were used as substrates. After sputtering, a metal contact system was deposited over the tin dioxide film by using thermal evaporation method. This contact system is consisted of two parallel strips 10 mm long with a gap between them of 0.1 mm.

2.2. Composition, structure and morphology study

The film morphology was estimated using the method of SEM-imaging of the cleaved film with a scanning electron microscope Mira II LMU (Tescan, Czech). The average grain size was estimated using the Gwyddion imaging software. Surface composition analysis and dopant thickness distribution was carried out by means of a scanning Auger electron spectroscopy and a secondary ion mass spectrometry with ion beam etching (Physical Electronics, PHI-4300, USA). Crystal structure was evaluated using a Xcalibur/Gemini A single crystal X-ray diffractometer (Oxford Diffraction, Poland, 2010). Also Raman spectra were analyzed using a highly sensitive confocal scanning Raman microscope (NTMDT, Zelenograd).

2.3. Gas-sensitivity study

The study of the response to acetone vapors and the long-term stability of the sensors were automatically performed using a measuring and computing system. System management was developed by means of a LabView environment. Test gas mixture was obtained using EL-FLOW flowmeters (Bronkhorst, Netherlands), that ensured measurement accuracy of ±1% of the full scale with a measurement time of less than 200 ms. Measurements were performed in a dry air flow with the rate of 100 ml/min. The sensor temperature was controlled using an "Erbium" temperature regulator. The sensor conductivity was measured by means a Keithley 2000-20 multipurpose tester. Schematic representation of a sensing element (a), photo of a holder for sensing element (b) and image of a measuring chamber (c) are presented in **Fig. 1.** The measuring chamber was a hollow aluminum (D16T) cylinder with an inner diameter of 18 mm and a height of 28 mm. The volume of the measuring chamber taking into account the volume displaced by the microthermostat and the sample was 5 cm3. Stagnant zones in the chamber were absent due to the special arrangement of the inlet and outlet fitting.

The characteristic purge time of the measuring chamber can be estimated by the formula:

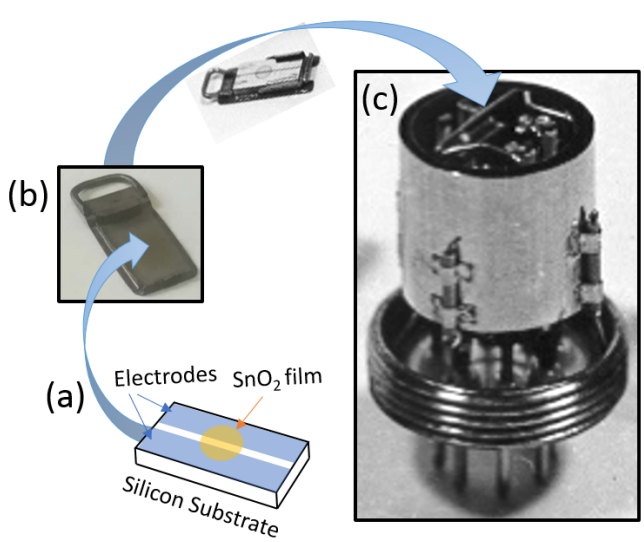

Fig. 1. *Schematic representation of a sensing element (a), photo of a holder for sensing element (b) and image of a measuring chamber (c).*

$$c(t) = (c_0 - c_{in})e^{-\frac{F}{V}t} + c_{in}, \quad (1)$$

where $c(t)$ is the dependence of the concentration of impurities in the measuring chamber on time, c_0 is the initial concentration of impurities in the chamber, cin is the impurity concentration in the gas entering the chamber, F is gas flow through the chamber, V is chamber volume. At a gas flow rate of 100 nml/min the typical purge time $\tau = V/F$ is less than 3s.

An admixture of acetone vapor was obtained by mixing saturated acetone vapor (370000 ppm at 25°*C*) with a stream of dry air in a ratio of 5/95 ml/min. The concentration of the acetone sample was 18500 ppm. Acetone vapors were obtained by sparging dry air through acetone. This method is common for obtaining impurities of substances that are in a liquid state at room temperature and have high volatility. The bubbler was a 1.5 liter glass container. The immersion depth of the sprayer and the air volume above water were 12 cm and 184 cm^3, respectively. The temperature of the acetone in the bubbler was kept constant at room temperature 25°*C*.

3. RESULTS AND DISCUSSION

3.1. Scanning electron microscopy.

An analysis of experimental films micrographs showed no dependence of films deposition rate on BiO_2 concentration in the target. The morphology of the all obtained films was similar one presented in **Fig. 2**.

The micrograph shows that the film consists of vertically oriented grains. The average grain size was calculated by statistical analysis of the obtained micrographs and was 21±2 nm for all samples. The film thickness was 120±10 nm. We decided to partially omit the energy dispersive analysis due to the small films thickness, comparable with the depth of signal generation, since small concentrations of bismuth cannot be identified against the background of the strong influence of a single-crystal silicon substrate. However, the content of tin and oxygen amounts about 30 mol.% and 70 mol.% respectively. The elements content corresponds to SnO2 stoichiometric ratio. A slight excess of oxygen may be attributed to the presence of silicon oxide on the substrate surface.

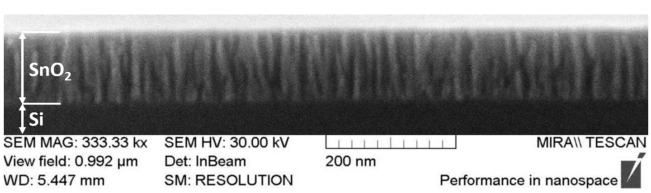

Fig. 2. *SEM - image of tin dioxide film cleavage morphology.*

3.2. Auger-spectroscopy

The chemical composition data of the surface obtained by the Auger electron spectroscopy method (AESM) is presented in **Table 1**. For comparison the data of Bi were also calculated by using molar ratio. The obtained results are also presented in Table 1. The content of target elements is converted from mass to atomic percentage for convenience. At BiO_2 concentration in the target value of 0.0063 at.% AESM did not reveal the presence of a dopant on the thin film surface. The Table 1 analysis has shown that the increase of concentration of BiO_2 in the target leads to decreasing the difference between concentration of Bi obtained by means molar ratio calculation and defined by AESM. It is expected that such trend related with the characteristics of films growth. The tin dioxide structure "expels" foreign atoms to the surface when concentration of the dopant element is low. Increase in the bismuth dioxide content in the target leads to deactivation of this mechanism, and the concentrations become the same.

Table 1

Sample content

Target composition		Sn, at.%	O, at.%	Bi, at% Molar calculation/ AESM
SnO_2, at%/масс.%	BiO_2, ат.%/масс.%			
100/100	0/0	48.59	51.41	0
99.9937/99.99	0.0063/0.01	49.88	50.12	0
99.937/99.9	0.063/0.1	48.67	51	0.021/0.32
99.37/99	0.63/1	47.44	50.8	0.21/1.76
93.7/90	6.3/10	46.73	46.96	2.1/6.3

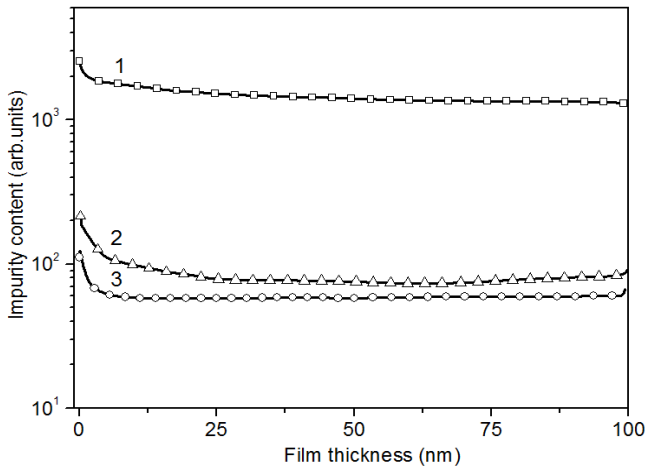

Fig. 3. *Distribution profile of Bi dopant over the tin dioxide film thickness. BiO_2 concentration in the target was 10 mass.% (1); 1 mass.% (2) and 0.1 mass.% (3).*

3.3. Secondary ion mass spectrometry

The approximated distribution profiles of the Bi dopant over the volume of a thin film are presented in **Fig. 3**. Results of the distribution of the dopant over the film volume evaluation are similar with Auger spectroscopy data. The signal strength at the start of sputtering is proportional to the bismuth concentration value figured out using Auger spectroscopy. For example, the signal level in a film with a bismuth concentration of 0.32 at.% corresponds to 120 arb. units, and concentration of 6.3 at.% - 2500 arb. units. In this way $6.3/0.32 \approx 2500/120 \approx 20$.

The decrease in the dopant content from sputtering time may be the result of decrease in the sputtering coefficient (dislodging of the surface atoms are more probable) either of decrease in the elements concentration. The latter, apparently, is driven by the crystal growth peculiarities, i.e. with the displacement of foreign impurities from the film structure.

3.4. Raman scattering spectroscopy

The Raman spectra of SnO_2 films doped with Bi at different BiO_2 concentrations in the target material is presented in **Fig. 4**. The peaks of silicon substrate significantly affect on the spectrum shape, due to the small thickness of the films. Therefore the figure demonstrates only a part of the spectrum.

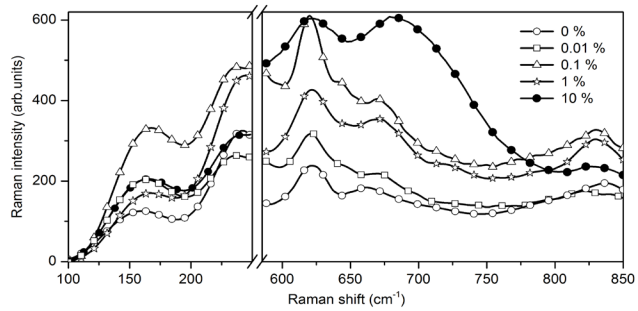

Fig. 4. *Raman spectrum of SnO_2 samples. BiO_2 concentration in target was 0 mass.%, 0.01 mass.%, 0.1 mass.%, 1 mass.%, 10 mass.%.*

There are no spectral peaks in the region of the Sn–O phase oscillation of tin oxide (approximately 211 cm^{-1} [29]). Small peaks are observed at wave numbers of 148 cm^{-1}, 237 cm^{-1}, and 245 cm^{-1}, that can be explained by the presence of nonstoichiometric tin dioxide phases, such as Sn_2O_3 and Sn_3O_4 [30-32]. Peaks in the interval of 615-640 cm^{-1} indicates the presence of the SnO_2 phase. According to [33] the peak location on the Raman spectrum near the 620 cm^{-1} depends on SnO_2 phase size. For bulk material, it is located at 632 cm^{-1}, while nanoparticles with dimensions of 7 nm and 25 nm have peaks at 621 cm^{-1} and 625 cm^{-1}, respectively. As can be seen in Fig. 3 all samples have pronounced peaks at 623 cm^{-1}, that indicates the presence of SnO_2 phase with an average size of nanoparticles approximately of 20 nm. This is coincided with the data obtained using an electron microscope. The Raman spectra of thick Bi films doped with SnO_2 nanoparticles were investigated in [34]. There was a peak at 660 cm^{-1} indicating bismuth concentration of ~3 mol.%, the value of which decreased with a decrease in bismuth concentration to 1 mol.%. Based on this facts, it is expected that the peaks at 670 cm^{-1} for samples with a content of BiO_2 0.1 wt.% and 1 wt.%, and 685 cm^{-1} for a sample with a content of 10 wt.% are probably associated with an increase in bismuth and its derivatives concentration in the film structure.

3.5. X-Ray diffraction

The X-ray patterns of the investigated SnO_2 films with different concentrations of BiO_2 in the target are shown in **Fig. 5**. The peaks on the radiographs of the films correspond to cassiterite form of SnO_2. The graphs are demonstrated a broadening and a slight shift of the diffraction reflections characteristic of SnO_2 with an increase in the mass content of BiO_2 in the target. On the one hand, bismuth introduction into the composition of the SnO_2 film can lead to an increase in the lattice constant due to the larger ionic radius compared to tin [35]. On the other hand, bismuth introduction can lead to an increase in the intrinsic defects concentration (oxygen vacancies) and a decrease in the lattice constant. For that matter, it is impossible to make firm conclusion about the inclusion of bismuth atoms in tin dioxide structure. The decrease in height and the broadening of diffraction reflections probably related with disturbance of the crystal structure of the material. Separate peaks corresponding to bismuth compounds were not detected.

3.6. Investigation of electrical properties of produced films

As is known, tin dioxide is a nonstoichiometric n-type semiconductor, in which oxygen vacancies are donor centers [32]. The diffusion of oxygen vacancies from the volume of polycrystalline samples onto the surface is activated at elevated temperatures. Oxygen vacancies associate with adsorbed oxygen on the surface of tin dioxide and lose its donor characteristics. Therefore a long-term change in the conductivity of the samples is observed at elevated temperatures.

The investigated samples conductivity drift was estimated at working temperature of 300°*C* in an atmosphere of dry air within 24 hours using an automated measuring system. The dynamics of changes in the conductivity of samples with various concentration of BiO_2 in the target are presented in **Fig. 6.** As it is seen in Fig. 6 introduction of bismuth dopant leads to a non-monotonic change in the samples conductivity in air. Initially conductivity is sharply increased then decreased and after some time to achieve a stationary value.

The drift value of samples conductivity was determined to estimate the long-term stability of the samples conductivity at elevated temperatures in air:

$$v_d = \frac{1}{\Delta t}\frac{G_4 - G_{24}}{G_4}100\%, \qquad (2)$$

where $\Delta t = 20h$ is the observation time of the change in the samples conductivity, G_4 and G_{24}

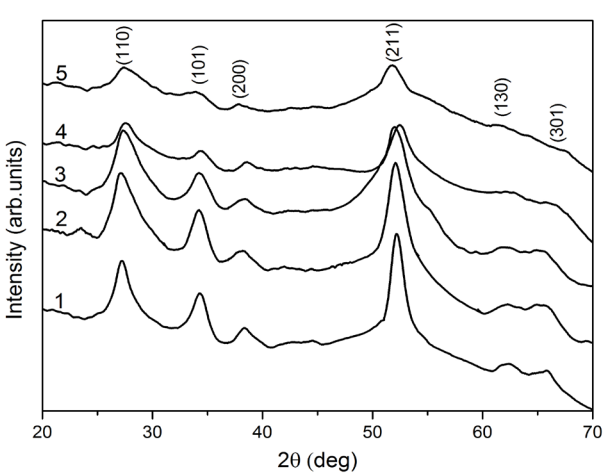

Fig. 5. *X-ray patterns of SnO_2 samples with different Bi concentration. BiO_2 concentration in target was 0 mass.%, 0.01 mass.%, 0.1 mass.%, 1 mass.%, 10 mass.%.*

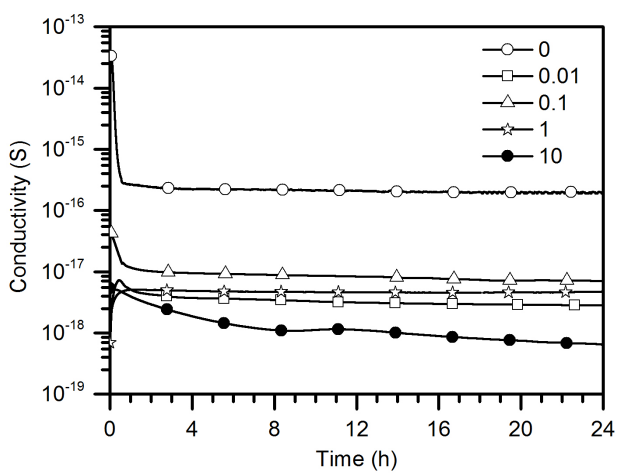

Fig. 6. *Time dependence of conductivity of SnO_2 film with different Bi concentration. BiO_2 concentration in target was 0 mass.%, 0.01 mass.%, 0.1 mass.%, 1 mass.%, 10 mass.%.*

are the conductivity values of samples after 4 hours and 24 hours after heating to a temperature of 300°*C*, respectively.

The results of the conductivity drift calculation are presented in **Fig. 7**. The lowest level of baseline drift was observed at the sample obtained by using a target with a BiO_2 content of 1 wt.%. It may be concluded that bismuth dopant introduction ambiguously affects the long-term stability of tin dioxide films conductivity. For samples obtained from a target with 1 wt.% BiO_2 concentration, the resistance drift decreased by a factor of 2 relative to the undoped sample. Apparently, the introduction of BiO_2 in amounts of less than 1 wt.% results in the originate of additional defects in the polycrystalline samples volume and an increase in conductivity drift value. A decrease in the long-term drift of conductivity when the concentration of BiO_2 in the target is 1 mass% may be due to the association of defects (oxygen vacancies) in a polycrystalline sample of tin dioxide and bismuth atoms. At the same time, the forming associative complexes (oxygen vacancies and bismuth dopant atoms) have a higher diffusion activation energy, which provides a decrease in the samples conductivity drift. Use of 10 mass% BiO_2 target in the doping of SnO_2 possibly leads to the formation of a polycrystalline composite material tin dioxide/bismuth oxide. In such samples, the long-term conductivity drift at elevated temperatures may be associated with the oxygen vacancies diffusion in grains of the tin dioxide phase, as well as with the processes of interphase diffusion of defects and dopant atoms along the grain boundaries.

The graph of the conductivity temperature dependence of SnO_2 samples is presented in **Fig. 8.** The temperature increase from 200°*C* to 350°*C* leads to samples conductivity increase, which indicates an activation mechanism for the conductivity change. Upon further heating, conductivity maximum is observed in the range of 370–420°*C*, and then a decrease in conductivity occurred (except for the sample obtained from 1 mass% and 10 mass% BiO_2 concentration target). Hysteresis in the temperature dependences of the samples conductivity is also observed, i.e. the heating curves pass below the cooling curves. The hysteresis value is different for various samples, and the sample obtained from a target with 0.1 mass% BiO_2 content in the target has a minimum hysteresis value.

The maximum in the temperature dependence of the SnO_2 samples conductivity is related to the adsorbed oxygen conversion from O_{2-} to O^- and O^{2-}. At operating temperatures of ~ 400°*C*, molecular oxygen in a neutral form adsorbed on the surface dissociates into atomic oxygen subsequently

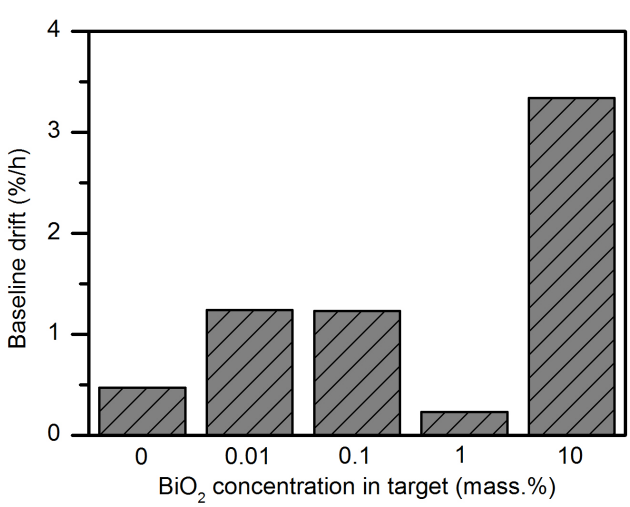

Fig. 7. *Dependence of conductivity drift on BiO_2 concentration in target.*

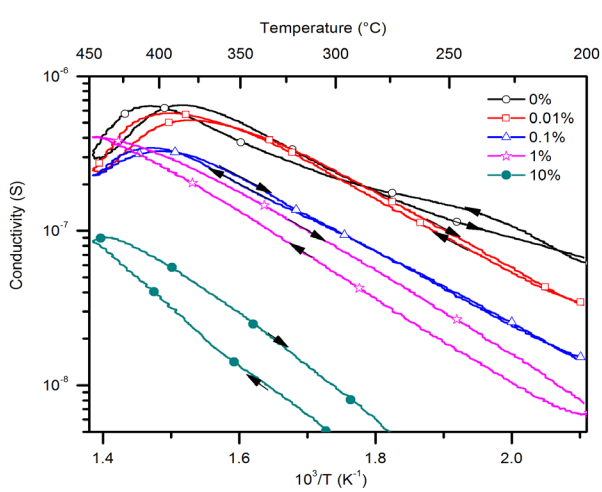

Fig. 8. *Temperature dependence of SnO_2 films resistance. BiO_2 concentration in target was 0 mass.%, 0.01 mass.%, 0.1 mass.%, 1 mass.%, 10 mass.%.*

capturing charge carriers (electrons) from the bulk of the grain. As a consequence, the samples conductivity decreases and a maximum of the temperature dependence of the conductivity is observed. It should be noted that the increase of BiO_2 concentration in the target of more than 1 wt.% results in disappearing of the maximum in the conductivity temperature dependence or in its shifting to the temperature range above 450°*C*. It can be assumed that the bismuth doping of the tin dioxide surface increases the dissociation energy of molecular oxygen adsorbed on its surface. In addition, the concentration of BiO_2 in the target of 0.1 wt.% and higher leads to a decrease in the tin dioxide samples conductivity, which can be ascribed to increase in the ionization degree of adsorbed oxygen due to the electron transfer from bismuth atoms to adsorbed oxygen atoms.

3.7. Investigation of gas-sensing properties of produced films

The time dependences of the films conductivity were obtained to analyze the effect of bismuth oxide concentration on the film response rate to acetone vapors in air. As an example, the dependence of the pure tin dioxide film conductivity on the exposure time of acetone vapor in air is presented in **Fig. 9**. The dependence indicates that the sample conductivity increased when the gas is introduced into the measuring chamber, and decreased when purging with purified air. Multiple repetition of the experiment shows that the conductivity of the film changes reversibly and reproduces with introduction of the analyzed samples. The response time (t_{res}) was about 7*s*. The recovery time (t_{rec}) significantly exceeded the response time and amounted to about 280*s* probably due to the high concentration of acetone vapor in the gas sample.

In the air, oxygen molecules adsorbing on the surface of tin dioxide capture electrons from the volume and charge negatively. Acetone molecules interact with ionized oxygen molecules and the products of the chemical interaction of acetone and oxygen are desorbed into the gas phase. Then electrons captured by adsorbed oxygen return to the bulk tin dioxide and the samples conductivity increases.

Fig. 10 presents the dependence of the response rate of tin dioxide samples formed from targets with different bismuth oxide concentration.

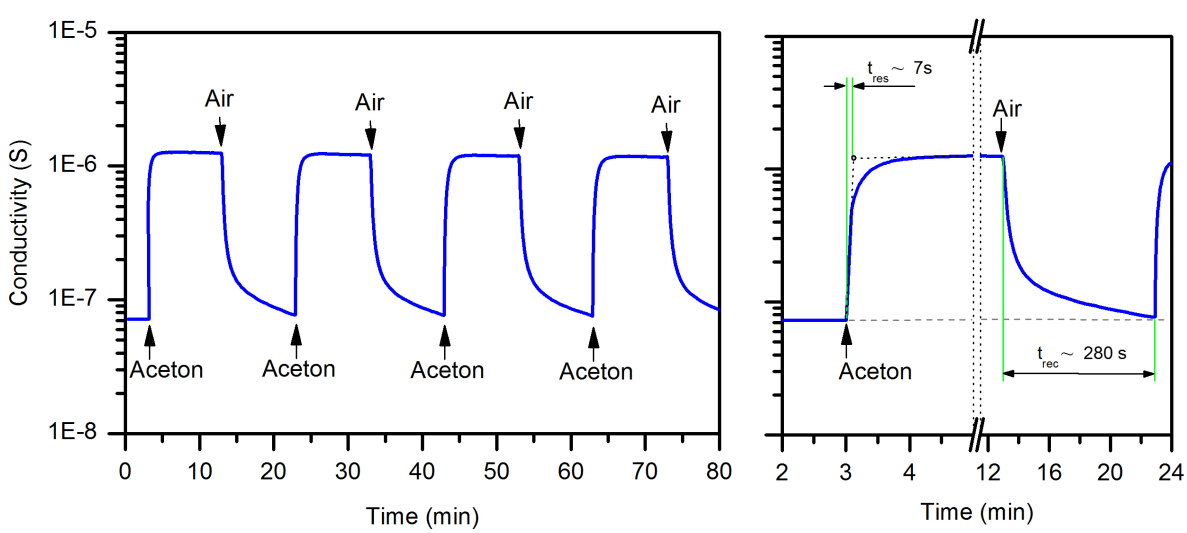

Fig. 9. *Dependence of gas sensor (based on pure SnO_2 film) conductivity on acetone exposure.*

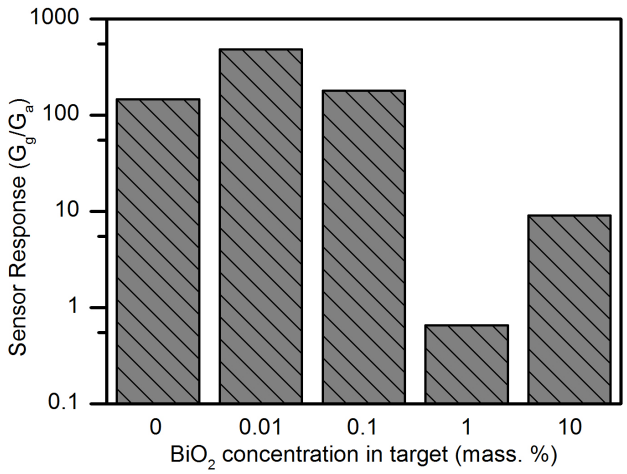

Fig. 10. *Dependence of SnO_2 film samples response rate on BiO_2 concentration in target material.*

The gas response (S) to gas samples exposure was evaluated as the ratio of conductivity in a gas sample (G_g) to conductivity in air (G_a):

$$S = G_g / G_a. \quad (3)$$

The highest response rate, equal to 850, was observed in samples with BiO_2 concentration in the target of 0.01 wt.% while samples with a concentration of 1% had the smallest response. A decrease in the response of samples with a BiO_2 content in the target of more than 0.1 wt.% can be attributed to the fact that amounts of the adsorbed oxygen is smaller on the tin dioxide surface in comparison with the surface of undoped samples. This fact is indicated by thermocycling data (Fig. 8). For that matter, when the gas samples are exposed, the amount of reacting oxygen with acetone molecules on the surface is less than in the case of low-alloyed and undoped samples.

Table 2 presents data on the response to high concentration of acetone for sensors based on pure SnO_2 and SnO_2 doped with various dopants. The data analysis shows that bismuth-doped tin dioxide films have good sensitivity and stability for development of acetone sensors.

Table 2

Comparison of the sensing properties of different SnO_2-based material toward acetone.

Material	Morphology	Acetone concentration (ppm)	Temperature (°C)	Sensitivity	t_{res}/t_{rec}	Ref.
Eu/SnO_2	Nanofibers	5000	280	520	4s/3s to 100 ppm	36
Au/SnO_2	Hollow microspheres	5000	220	720	0.9s/21s to 5 ppm	37
SnO_2	Aurelia-like micronanostrucrture	3000-5000	240	140	2s/23s to 100 ppm	38
Y/SnO_2	Hollow nanofibers	8000	300	550	30s/9s to 500 ppm	39
Ce/SnO_2	Nanoparticles	15000-20000	270	1250	200s/575s to 50 ppm	40
Bi/SnO_2	Thin film	18500	300	850	7s/280s to 18500 ppm	Our work
ZnO/SnO_2	Heteronanofibers	40000	300	1350	19s/9s to 100 ppm	41
SnO_2	Nanobelts	30000-50000	260	1000	38s/9s to 100 ppm	42

4. CONCLUSION

The effect of various concentrations of bismuth dopant on the morphology, chemical composition and structure of tin dioxide films was studied. Peculiarities of the dopant distribution over the experimental film thickness were identified. It was found out, that the films composed of crystalline rods directed transversely to the substrate surface, with diameter and length of 20-21 nm and 120±10 nm, respectively. It was demonstrated, that the sensitivity to saturated acetone vapors increases by almost 10 times (up to 850) for a sample formed from a target with a bismuth oxide concentration of 0.01%, compared to an undoped film. Baseline drift of the most sensitive samples increased from 0.47%/hour for the undoped sample to 1.24%/hour for the doped sample. This fact indicates the necessity for annealing of the doped samples after obtaining, in order to relieve mechanical stresses in the growing structure.

In general, evaluated data shows prospects of bismuth-doped tin dioxide films usage for producing the saturated acetone vapor sensors.

REFERENCES

1. Batzil M. Surface science studies of gas sensing materials:SnO_2. *Sensors,* 2006, 6:1345-1366.
2. Korotcenkov G, Brinzari V, Pronin IA, Ham MH, Cho BK. Metal oxides for application in conductometric gas sensors: how to choose?, *Solid State Phenomena,* 2017, 266:187-195.
3. Singh G, Virpal, Singh RC. Highly sensitive gas sensor based on Er-doped SnO_2 nanostructures and its temperature dependent selectivity towards hydrogen and ethanol. *Sensors and Actuators B: Chemical,* 2019, 282:373-383.
4. Lin FZ.D , Li N, Chen Z, Fu P. The effect of Ni doping concentration on the gas sensing properties of Ni doped SnO_2. *Sensors and Actuators B: Chemical*, 2017, 239:501-510.
5. Chen Y, Yu L, Feng D, Zhuo M, Zhang M, Zhang E, Xu Z, Li Q, WangT. Superior ethanol-sensing properties based on Ni-doped SnO_2 p–n heterojunction hollow spheres. S*ensors and Actuators B: Chemical,* 2012*,* 166:61-67.
6. Singh D, Kundu VS, Maan AS. Structural, morphological and gas sensing study of zinc doped tin oxide nanoparticles synthesized via hydrothermal technique. *Journal of Molecular Structure,* 2016, 1115:250-257.
7. Lin Y, Wang Y, Wei W, Zhu L, Wen S, Ruan S. Synergistically improved formaldehyde gas sensing properties of SnO_2 microspheres by indium and palladium co-doping. *Ceramics International*, 2015, 41:7329-7336.
8. N. Murata, T. Suzuki, M. Kobayashi, F. Togoh, K. Asakura. Characterization of Pt-doped SnO_2 catalyst for a high-performance micro gas sensor. *Physical Chemistry Chemical Physics*, 2013, 41:17938-17946.
9. W. Chen, Q. Zhou, T. Gao, X. Su, F. Wan. Pd-doped SnO_2-based sensor detecting characteristic fault hydrocarbon gases in transformer oil. *Journal of Nanomaterials*, 2013, 127345.
10. Y. Lin, W. Wei, Y. Li, F. Li, J. Zhou, D. Sun, Y. Chen, S. Ruan. Preparation of Pd nanoparticle-decorated hollow SnO_2 nanofibers and their enhanced formaldehyde sensing properties. *Journal of Alloys and Compaunds*, 2015, 651:690-698.
11. G. Korotcenkov, B.K. Cho, L. Gulina, V. Tolstoy. SnO2 thin films modified by the SnO_2–Au nanocomposites: response to reducing gases. *Sensors and Actuators B: Chemical*, 2009, 141:610-616.
12. L. Xiao, S. Shu, S. Liu. A facile synthesis of Pd-doped SnO_2 hollow microcubes with enhanced sensing performance. *Sensors and Actuators B: Chemical,* 2015, 221:120-126.
13. C. Li, Z. Yu, S. Fang, S. Wu, Y. Gui, R. Chen. Synthesis and gas-sensing properties of Ce-doped SnO_2 materials. *Journal of Physics: Conference Series,* 2009, 152:012033.
14. P. Mohanapriya, S. Hiroyo, K. Watanabe, S. Samitsu, T.S. Natarajan, N.V. Jaya, N. Ohashi. Enhanced ethanol-gas sensing performance of Ce-doped SnO_2 hollow nanofibers prepared by electrospinning. *Sensors and Actuators B: Chemical,* 2013, 188:872-878.
15. D. Liu, T. Liu, H. Zhang, C. Lv, W. Zeng, J. Zhang. Gas sensing mechanism and properties of Ce-doped SnO_2 sensors for volatile organic compounds. *Materials Science in Semiconductor Processing,* 2012, 15:438-444.
16. W. Chen, Q. Zhou, L. Xu, F. Wan, S. Peng, W. Zeng. Improved methane sensing properties of Co-doped SnO_2 electrospun nanofibers. *Journal of Nanomaterials*, 2013, 173232.
17. K.M. Kim, K.-I. Choi, H.-M. Jeong, H.-J. Kim, H.-R. Kim, J.-H. Lee. Highly sensitive and selective trimethylamine sensors using Ru-doped SnO_2 hollow spheres. *Sensors and Actuators B: Chemical*, 2012, 166:733-738.
18. Z. Lou, L. Wang, T. Fei, T. Zhang. Enhanced ethanol sensing properties of NiO-doped SnO_2 polyhedra. New Journal of Chemistry, 2012, 36:1003-1007.

19. Z. Wang, L. Liu. Synthesis and ethanol sensing properties of Fe-doped SnO_2 nanofibers. *Materials Letters,* 2009, 63:917-919.
20. S.I. Rembeza, N.N. Kosheleva, E.S. Rembeza, T.V. Svistova, Y.V. Shmatova, G. Xu. Electrical and gas-sensitive properties of nanostructured SnO_2:ZrO_2 semiconductor films. *Semiconductors,* 2011, 45:603-606.
21. W.X. Jin, S.Y Ma, Z.Z. Tie, J.J. Wei, J. Luo, X.H. Jiang, T.T. Wang, W.Q. Li, L. Cheng, Y.Z. Mao. One-step synthesis and highly gas-sensing properties of hierarchical Cu-doped SnO_2 nanoflowers. *Sensors and Actuators B: Chemical,* 2015, 213:171-180.
22. J. Tamaki, K. Shimanoe, Y. Yamada, Y. Yamamoto, N. Miura, N. Yamazoe. Dilute hydrogen sulfide sensing properties of CuO-SnO_2 thin film prepared by low-pressure evaporation method. *Sensors and Actuators B: Chemical*, 1998, 49:121-125.
23. M.N. Rumyantseva, M. Labeau, J.P. Senateur, G. Delabouglise, M.N. Boulova, A.M. Gaskov. Influence of copper on sensor properties of tin dioxide films in H_2S. *Materials Science and Engineering: B-Advanced Functional Solid State Materials,* 1996, 41:228-234.
24. W. Zhang, B. Yang, J. Liu, X. Chen, X. Wang, C. Yang. Highly sensitive and low operating temperature SnO_2 gas sensor doped by Cu and Zn two elements. *Sensors and Actuators B: Chemical*, 2017, 243:982-989.
25. V.V. Kissine, V.V. Sysoev, S.A. Voroshilov. A comparative study of SnO_2 and SnO_2:Cu thin films for gas sensor applicationsıo *Thin Solid Films,* 1999, 348:304-311.
26. C.S. Rastomjee, R.S. Dale, R.J. Schaffer, F.H. Jones, R.G. Egdell, G.C. Georgiadis, M.J. Lee, T.J. Tate, L.L. Cao. An investigation of doping of SnO_2 by ion implantation and application of ion-implanted films as gas sensors. *Thin Solid Films*, 1996, 279:98-105.
27. R.S. Dale, C.S. Rastomjee, F.H. Potter, R.G. Egdell, T.J. Tate. Sb and Bi implanted SnO_2 thin films: photoemission studies and application as gas sensors. *Applied Surface Science*, 1993, 70:359-362.
28. J.H. Bang, M.S. Choi, A. Mirzaei, Y.J. Kwon, S.S. Kim, T.W. Kim, H.W. Kim. Selective NO_2 sensor based on Bi2O3 branched SnO_2 nanowires. *Sensors and Actuators B: Chemical,* 2018, 274:356-369.
29. E.L.P. Blancá, B. Peltzer, Y. Peltzer, E.L. Blanc, A. Svane, N.E. Christensen, C.O. Rodriguez, O.M. Cappannini, M.S. Moreno, Calculated static and dynamic properties of -Sn and Sn-O compounds. *Physical Review B*, 1993, 48:15712.
30. Y. Zhu, Y. Chen, X. Zhang. Study on the annealing-dependent photoluminescence properties of SnO_2 cluster-system structures. *European Journal of Chemistry,* 2011, 2:8-13.
31. I.A. Zhurbina, O.I. Tsetlin, V.Y. Timoshenko. Optical generation of free charge carriers in thin films of tin oxide. *Semiconductors*, 2011, 45:236-240.
32. M. Batzill, U. Diebold. The surface and materials science of tin oxide. *Progress in Surface Science,* 2005, 79:47-154.
33. V.G. Kravets. Photoluminescence and Raman spectra of SnO_x nanostructures doped with Sm ions. *Optics and Spectroscopy,* 2007, 103:766-771.
34. L.P. Chikhale, J.Y. Patil, F.I. Shaikh, A.V. Rajgure, R.C. Pawar, I.S. Mulla, S.S. Suryavanshi. Effect of Bi doping on structural, morphological, optical and ethanol vapor response properties of SnO_2 nanoparticles. *Materials Science in Semiconductor Processing*, 2014, 27:121-129.
35. Wells AF. *Structural inorganic chemistry.* Clarendon Press, Oxford, 1975, 1127 p.
36. Z.Q. Jiang, R. Zhao, B.L. Sun, G.D. Nie, H. Ji, J.Y. Lei, C. Wang. Highly sensitive acetone sensor based on Eu-doped SnO_2 electrospun nanofibers. *Ceramics International,* 2016, 42:15881–15888
37. Y. Li, L. Qiao, D. Yan, L. Wang, Y. Zeng, H. Yang. Preparation of Au-sensitized 3D hollow SnO_2 microspheres with an enhanced

sensing performance. *Journal of Alloys and Compounds,* 2014, 586:399-403.

38. H. Yu, S. Wang, C. Xiao, B. Xiao, P. Wang, Z. Li, M. Zhang. Enhanced acetone gas sensing properties by aurelia-like SnO_2 micronanostructures. *Crystengcomm*, 2015, 17:4316.
39. L. Cheng, S.Y. Ma, S.Y. Li, J. Luo, W.Q. Li, F.M. Li, Y.Z. Mao, T.T. Wang, Y.F. Li. Highly sensitive acetone sensors based on Y-doped SnO_2 prismatic hollow nanofibers synthesized by electrospinning. *Sensors and Actuators B: Chemical,* 2014, 200:181–190.
40. X. Lian, Y. Li, X. Tong, Y. Zou, X. Liu, D. An, Q. Wang. Synthesis of Ce-doped SnO_2 nanoparticles and their acetone gas sensing properties. *Applied Surface Science,* 2017, 407:447-455.
41. S.H. Yan, S.Y. Ma, X.L. Xu, W.Q. Li, J. Luo, W.X. Jin, T.T. Wang, X.H. Jiang, Y. Lu, H.S. Song. Preparation of SnO_2-ZnO hetero-nanofibers and their application in acetone sensing performance. *Materials Letters,* 2015, 159:447–450.
42. W.Q. Li, S.Y. Ma, J. Luo, Y.Z. Mao, L. Cheng, D.J. Gengzang, X.L. Xu, S.H. Yan. Synthesis of hollow SnO_2 nanobelts and their application in acetone sensor. *Materials Letters,* 2014, 132:338-341.